INTERNATIONAL JOURNAL FOR NUMERICAL METHODS IN FLUIDS
Int. J. Numer. Meth. Fluids 2005; **49**:331–348
Published online 9 June 2005 in Wiley InterScience (www.interscience.wiley.com). DOI: 10.1002/fld.1014

Effects of free-stream turbulence on large-scale coherent structures of separated boundary layer transition

Zhiyin Yang[1,*,†] and Ibrahim E. Abdalla[2,‡]

[1]*Department of Aeronautical and Automotive Engineering, Loughborough University, Loughborough LE11 3TU, U.K.*
[2]*Institute of Energy and Sustainable Development, De Montford University, Leicester LE1 9BH, U.K.*

SUMMARY

It has been well established that large-scale structures, usually called coherent structures, exist in many transitional and turbulent flows. The topology and range of scales of those large-scale structures vary from flow to flow such as counter-rotating vortices in wake flows, streaks and hairpin vortices in turbulent boundary layer. There has been relatively little study of large-scale structures in separated and reattached transitional flows.

Large-eddy simulation (LES) is employed in the current study to investigate a separated boundary layer transition under 2% free-stream turbulence on a flat plate with a blunt leading edge. The Reynolds number based on the inlet free stream velocity and the plate thickness is 6500. A dynamic subgrid-scale model is employed to compute the subgrid-scale stresses more accurately in the current transitional flow case. Flow visualization has shown that the Kelvin–Helmholtz rolls, which have been so clearly visible under no free-stream turbulence (NFST) are not as apparent in the present study. The Lambda-shaped vortical structures which can be clearly seen in the NFST case can hardly be identified in the free-stream turbulence (FST) case. Generally speaking, the effects of free-stream turbulence have led to an early breakdown of the boundary layer, and hence increased the randomization in the vortical structures, degraded the spanwise coherence of those large-scale structures. Copyright © 2005 John Wiley & Sons, Ltd.

KEY WORDS: large-eddy simulation; large-scale structures; coherent structures

1. INTRODUCTION

It has been found that spatially coherent and temporally evolving vortical structures, popularly called *coherent structures* (CS) [1], exist in turbulent shear flows. The presence of CS

*Correspondence to: Zhiyin Yang, Department of Aeronautical and Automotive Engineering, Loughborough University, Loughborough LE11 3TU, U.K.
†E-mail: Z.Yang@lboro.ac.uk
‡E-mail: IAbdalla@dmu.ac.uk

Contract/grant sponsor: EPSRC

Received 13 December 2004
Revised 6 May 2005
Accepted 10 May 2005

in turbulent shear flows was first suggested by Townsend [2] but they were also noticed in the early experiments of Corrsin [3]. Those structures seem to be strongly dependent on the flow geometry, the flow condition and the location with respect to solid surfaces. For example, large-scale spanwise vortices appear to dominate the dynamics in plane mixing layer [4]. On the other hand, dominant structures of the transitional plane boundary layer may be a Lambda-shaped vortex and low-speed streaks [5]. In wakes, counter-rotating vortices are known to dominate the flow dynamics too [6].

Understanding the evolution and interaction of CS and coupling of CS with background turbulence is very important not only for having a better insight into turbulence phenomena such as entrainment and mixing, heat and mass transfer, chemical reaction and combustion, drag and aerodynamic noise generation, but also for viable modelling of turbulence [7]. Therefore, a wide range of investigations have been carried out to try to have a better understanding of CS and their dynamical roles in turbulence. The starting point is, of course, to identify CS in different flow situations. Generally speaking, the following five methods can be used to identify CS:

1. Wavelets.
2. Conditional sampling (VITA, LSE).
3. Pattern recognition.
4. Proper orthogonal decomposition POD.
5. Flow visualization.

Flow visualization with recourse to large-eddy simulation (LES) has been used in the present study, and hence the other four methods will not be discussed here and can be found elsewhere [5, 6, 8–10].

Flow visualization has been traditionally used to reveal flow structures. However, it is not a very objective method because how well and how clearly the flow structures can be shown depends on the visualization schemes used. A high vorticity modulus, Ω, is a possible candidate for coherent-vortex identification, especially in free shear flows. For instance, Comte *et al.* [11] extensively discussed the dynamics of streamwise vortices in mixing layer on the bases of Ω-isosurfaces. In the presence of a wall, however, the mean shear created by the no-slip condition is usually significantly higher than the typical intensity of the near-wall vortices. A more sophisticated criterion is therefore required to distinguish vortices from internal shear layers in those types of flows.

Low-pressure isosurfaces have been used by Comte *et al.* [11] in their investigation of CS in a turbulent boundary layer, indicating the superiority of pressure as a vortex visualization criterion rather than the vorticity modulus. However, in regions of high concentration of vortices, this criterion may fail to capture the details of the vortical structures.

A criterion which shares some properties with both the vorticity and the low-pressure isosurface is the Q-criterion named after the second invariant of velocity gradient tensor by Hunt *et al.* [12].

In the current study a blunt plate is kept parallel to an on coming stream with 2% turbulence level. The flow separates at the leading edge and reattaches on the surface of the plate at a downstream location. There have been a few experimental studies on the effect of free-stream turbulence (FST) on separated and reattached flows. Saathoff and Melbourne [13] studied the cause of large pressure fluctuation near the leading edges of sharp-edged bluff bodies in the presence of FST. Measurements show that very low pressure occurs in a narrow

region located about $0.25x_R$ from the leading edge, where x_R is the mean reattachment length. From the visualization they concluded that the process is initiated when a perturbation in the approaching flow causes a roll-up of the separated shear layer, producing a strong vortex near the surface. Hillier and Cherry [14] showed that the mean separation bubble length was insensitive to turbulence length scale and Nakamura and Ozono [15] reached similar conclusion after exploring the effect of turbulence length scales over a wider range. However, the FST intensity has a major impact on the mean bubble length and their results indicate that increasing FST level is to produce considerable contraction of the bubble length. Kalter and Fernholz [16] experimentally investigated the effect of FST on a boundary layer with an adverse pressure gradient and a closed reverse-flow region. They found that by adding FST the mean reverse-flow region was shorten or completely eliminated, a method they believe can be used to control the size of the separation bubble.

Visualizations of the behaviour of large-scale structures from those experimental studies are very limited. Very few LES and DNS studies on the effect of FST on separated boundary layer transition have been carried out, especially regarding the effect of FST on the large-scale structures. Abdalla and Yang [17] have presented the large-scale CS for the no free-stream turbulence (NFST) case and the objective of this paper is to identify if there are similar large-scale structures in the FST case as in the NFST case, the effects of FST on the structures and on the transition process.

2. NUMERICAL PROCEDURE

The numerical methods employed in the current studies are direct descendants of well-known finite-volume techniques successfully used for many high-Reynolds-number LES studies, and recently for separated boundary layer transition on a flat plate with a semi-circular leading edge by Yang and Voke [18]. The velocity components at the grid points are interpreted as the volume average. Any small-scale (smaller than the control volume) motions are averaged out and have to be accounted for by a subgrid-scale model. A standard dynamic subgrid-scale model in Cartesian co-ordinates is used in the present study. The explicit second-order Adams–Bashforth scheme is used for the momentum advancement. The Poisson equation for pressure is solved using an efficient hybrid Fourier multigrid method. The spatial discretization scheme is the second-order central differencing which is widely used in LES owing to it is non-dissipative and conservative properties. More details of the mathematical formulation and numerical methods have been reported elsewhere by Yang and Voke [19].

Figure 1 shows the computational domain and mesh used in the present study. The study on the mesh refinement has been done for the NFST case with two simulations performed to make sure that the results are reliable and not dependent on the grid size [17]. Since the present study (FST case) has the same geometry and the same Reynolds number as in the NFST case so that the finer mesh used in the NFST case is adequate for the current FST case. The grid is consisting of $256 * 212 * 64$ cells along the streamwise, wall-normal and spanwise directions, respectively. The origin of the x-coordinate is located $0.5D$ from the leading edge of the plate. The inflow boundary is at 4.5 plate thickness ($D = 10.0\,\text{mm}$) from the plate leading-edge ($x_{in} = -5D$) while the outflow boundary is at $20.5D$ from the leading edge ($x_{out} = 20D$). The lateral boundaries are at $8D$ away from the plate surface, corresponding to a blockage ratio of 16. The spanwise dimension of the domain is 4D. Yang and Voke [18]

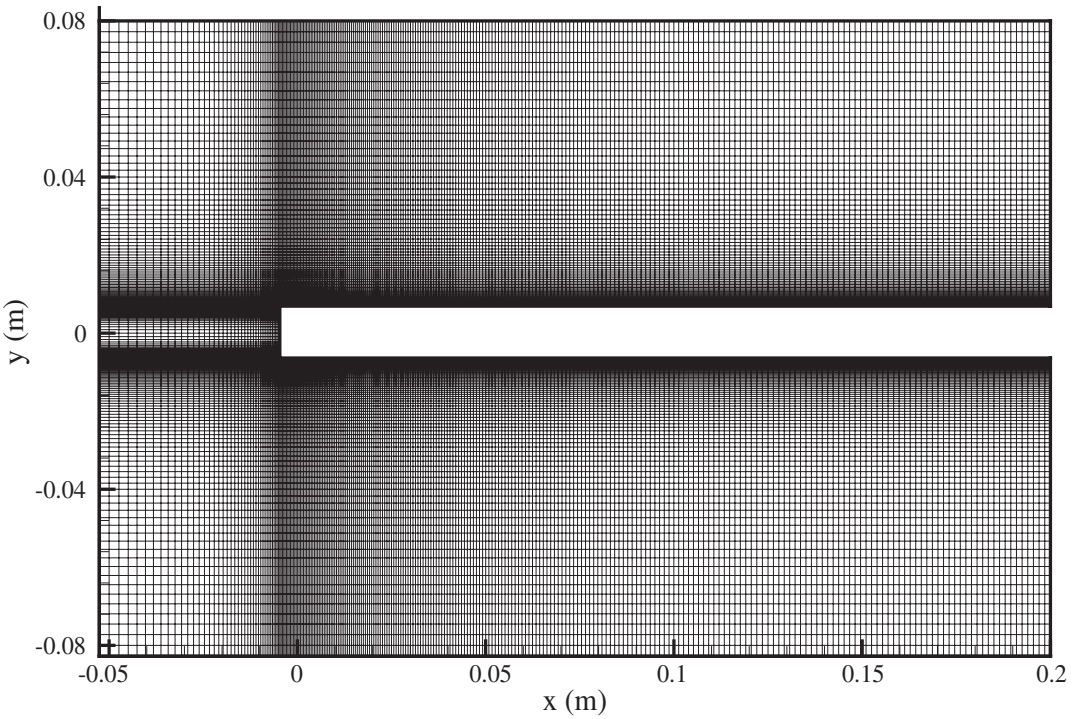

Figure 1. Computational domain and mesh in the x–y plane.

did a study on the effects of the location of the spanwise, periodic planes (two spanwise dimensions were used, 2D and 4D) in a very similar type of flow (flow over a flat plate with a semi-circular leading edge) and did not find any appreciable change in the behaviour of the flow (less than 5% difference in terms of averaged statistics for both mean and turbulence stress). In terms of wall units based on the friction velocity downstream of reattachment at $x/x_R = 2.5$, the streamwise mesh sizes vary from $\Delta x^+ = 9.7$ to $\Delta x^+ = 48.5$, $\Delta z^+ = 20.2$ and at the wall $\Delta y^+ = 2.1$, justifying the use of no-slip wall boundary condition. The time step used in this simulation is $0.001885D/U_0$. The simulation ran for 91 400 time steps to allow the transition and turbulent boundary layer to become established, i.e. the flow has reached a statistically stationary state, and the averaged results were gathered over further 159 990 steps, with a sample taken every 10 time steps (15 999 samples) and averaged over the spanwise direction too, corresponding to around 11 flow-through or residence times. The computations were carried out on Cray T3E using 16 processors most of the time. The RAM required was about 2 Gb and it took about a total of 1500 CPU hours. The code is highly efficient as the Poisson equation for pressure is solved using a hybrid Fourier multigrid, which results in a speed-up of at least 5 times compared with a fully 3D Poisson solver. This indicates that LES of more complicated turbulent flows in fully 3D geometry, i.e. periodic boundary conditions cannot be applied in spanwise directions, and hence Fourier transform cannot be employed to speed up the computations, is still very computationally demanding.

A free-slip but impermeable boundary condition (velocity normal to the boundary is zero and the gradient of velocities parallel to the boundary is also set to be zero) is applied on the lateral boundaries. Since the lateral boundaries are $8D$ away from the plate surface, and hence flow near the boundary region is very calm and parallel to the plate (laminar flow region) so that the boundary condition used has little influences on the results. In the spanwise direction the flow is homogeneous, and hence periodic boundary conditions are used. No-slip boundary conditions are used at solid walls. At the outflow boundary a convective (also known as non-reflective) boundary condition is applied, i.e. $(\partial U_i/\partial t) + C(\partial U_i/\partial x) = 0$. U_i represents three velocity components and C is taken to be a constant convection velocity, which is the averaged velocity at outlet boundary in the present study. A constant and sensible value of C such as the averaged velocity yields satisfactory results for incompressible flows but efforts are needed to determine an optimal C-value to ensure non-reflecting behaviour in compressible and aeroacoustics computations [20]. Non-uniform grid distributions are used in the x- and y-directions with finer resolution in the vicinity of the flat plate to resolve the shear layer. A uniform grid distribution is used in the spanwise direction. Realistic turbulence has to be prescribed at the inflow boundary to mimic FST which is very difficult to generate numerically. The LES and DNS community has been concerned with this enigma for a long time. Up to date there are no universal efficient methods that can be used to generate inflow data to simulate turbulence realistically despite many investigations. Several methods have been tried in the present study but they are not very satisfactory. As a result, the so-called 'precursor technique' is employed, i.e. an additional channel flow simulation has been performed, to provide realistic turbulent inflow data with 2% free-stream turbulence intensity.

3. RESULTS AND DISCUSSION

3.1. Mean variables

An important parameter characterizing a separated and reattached flow is the mean separation bubble length. The predicted mean bubble length for the current FST case is $5.6D$ while for the NFST case it is $6.5D$, leading to 14% reduction due to 2% FST. It is a well-known fact that the mean separation bubble length can be substantially reduced by the FST as found experimentally [14–16]. The current results are consistent with the experimental results.

Figure 2 compares the predicted mean streamwise velocity profiles (for both the FST and NFST cases, normalized by the free stream velocity) with the experimental data by Kiya and Sasaki [21] at five streamwise locations. The experiment was carried out with very low FST level but at much higher Reynolds number (26 000) and the measured reattachment length was about $5D$. The mean reattachment length is Reynolds number dependent as Djilali and Gartshore [22] reported a value of about $4.7D$ at a much higher Reynolds number (50 000). Numerically, several factors could affect the predicted bubble length such as subgrid-scale models, which is demonstrated by Suksangpanomrung *et al.* [23] using three different subgrid-scale models. To facilitate comparisons the profiles are plotted as function of y/x_R at corresponding values of x/x_R, i.e. comparisons are made at the same non-dimensionalized location (x/x_R) but not at the same geometric location (x). The LES results in both cases show a reasonably good agreement with the experimental data. The predicted peak and the free stream values of the velocity are bigger than those measured by Kiya and Sasaki [21].

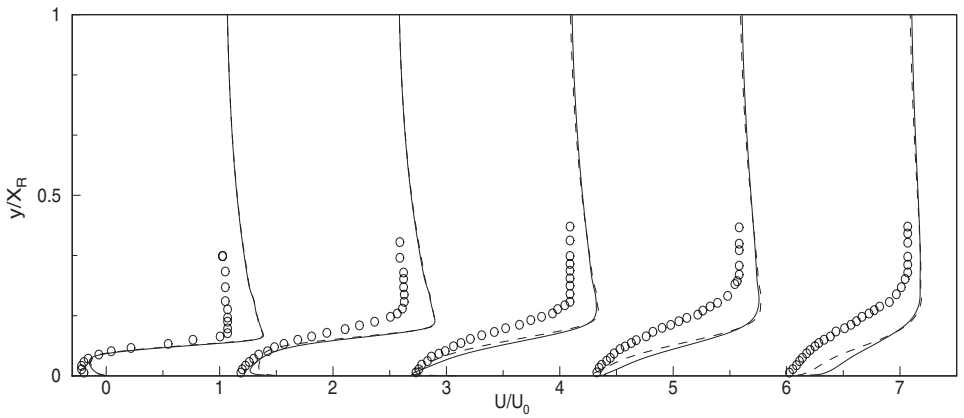

Figure 2. Mean axial velocity profiles at five streamwise locations measured from the leading edge. Left to right, $x/x_R = 0.2, 0.4, 0.6, 0.8, 1.0$. Solid line, LES (FST case); dashed line, LES (NFST case); symbols, experimental data.

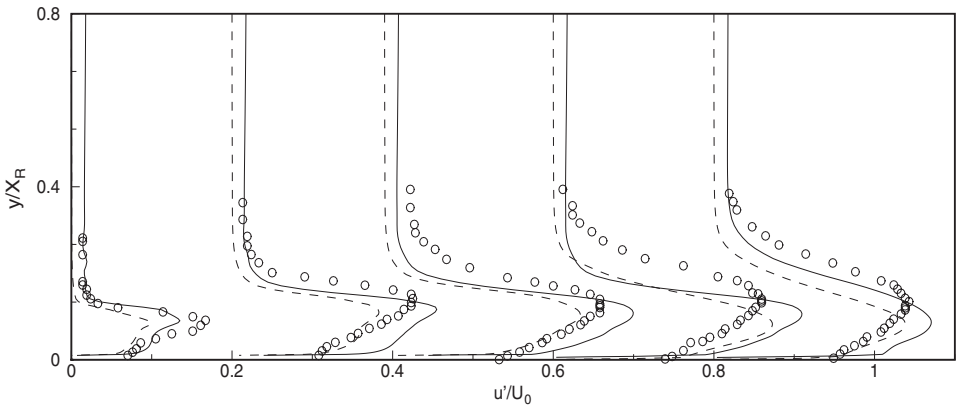

Figure 3. Axial velocity fluctuations rms profiles at five streamwise locations measured from the leading edge. Left to right, $x/x_R = 0.2, 0.4, 0.6, 0.8, 1.0$. Solid line, LES (FST case); dashed line, LES (NFST case); symbols, experimental data.

This discrepancy could be due to the differences in blockage ratio (20 in the experiment and 16 in the current study), due to the Reynolds number differences (26 000 in the experiment and 6500 in the current study) and also due to the fact that it was turbulent separation at the leading edge in the experiment while it is laminar separation in the current study. The results for both the FST and the NFST cases are very similar which indicates that 2% FST does not have a noticeable impact on the mean velocity.

Figure 3 shows profiles of the rms of streamwise velocity normalized by U_0 at the same five streamwise locations. The effect of free-stream turbulence can be clearly seen in this figure as the results in the FST case show not only higher values far away from wall in the

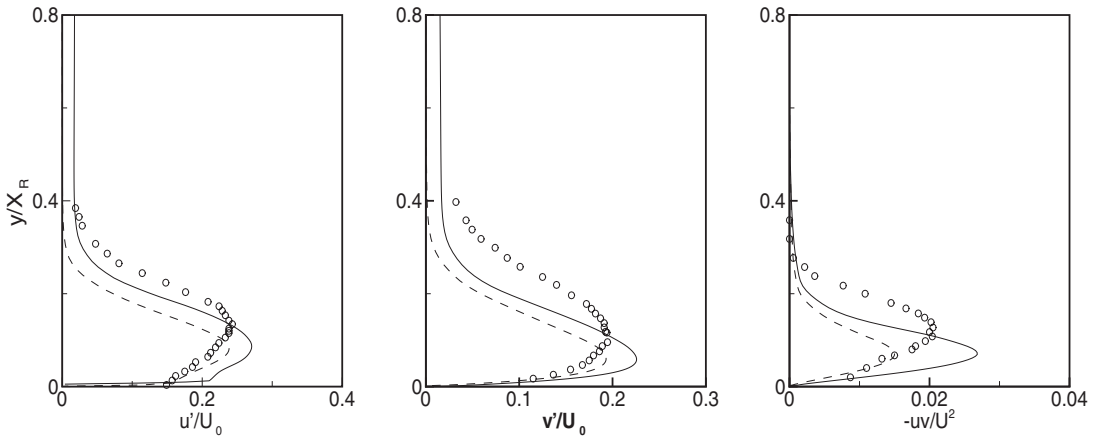

Figure 4. Velocity fluctuations rms and Reynolds shear stresses at the mean reattachment location. Solid line, LES (FST case); dashed line, LES (NFST case); symbols, experimental data.

free-stream but also higher peak values near the wall compared with the results in the NFST case. At the first two stations the FST results agree better with the experimental data than the NFST results, indicating that transition may occur earlier when the free-stream turbulence is present. However, at the other three stations the FST results show a slightly higher peak value compared with the experimental data whereas the NFST results agree slightly better with the experimental data in the near-wall region.

Figure 4 shows the comparison between the predicted u_{rms}, v_{rms} and $-uv$ with the experimental data by Kiya and Sasaki [21] at the mean reattachment point. The predicted results in the FST case give slightly higher values for u_{rms} and v_{rms} compared with the results in the NFST case. A good agreement has been obtained between the LES results in both cases and the experimental data for u_{rms} and v_{rms}. However, there is larger discrepancy between the predicted results and the experimental data for $-uv$ as it is overpredicted in the FST case and underpredicted in the NFST case. The effect of FST can be still seen at this streamwise location where transition has more or less finished.

3.2. Transition process

Figure 5 shows a snap shot of the instantaneous spanwise vorticity in the x–y plane for the NFST case (a) and FST case (b) at the mid-span location. The transition process is clearly visible from this figure. Flow separates at the leading edge and a free shear layer develops with 2D spanwise vortices formed. The free shear layer is inviscidly unstable via the Kelvin–Helmholtz mechanism and any small disturbances present grow downstream with an amplification rate larger than that in the case of viscous instabilities. Further downstream, the initial spanwise vortices are distorted severely and roll-up, leading to streamwise vorticity formation associated with significant 3D motions, eventually breaking down into relatively smaller turbulent structures at about the reattachment point and developing into a turbulent boundary layer rapidly afterwards. The transition process for both the FST case and NFST case seems to be quite similar but in the FST case the transition and the breakdown of

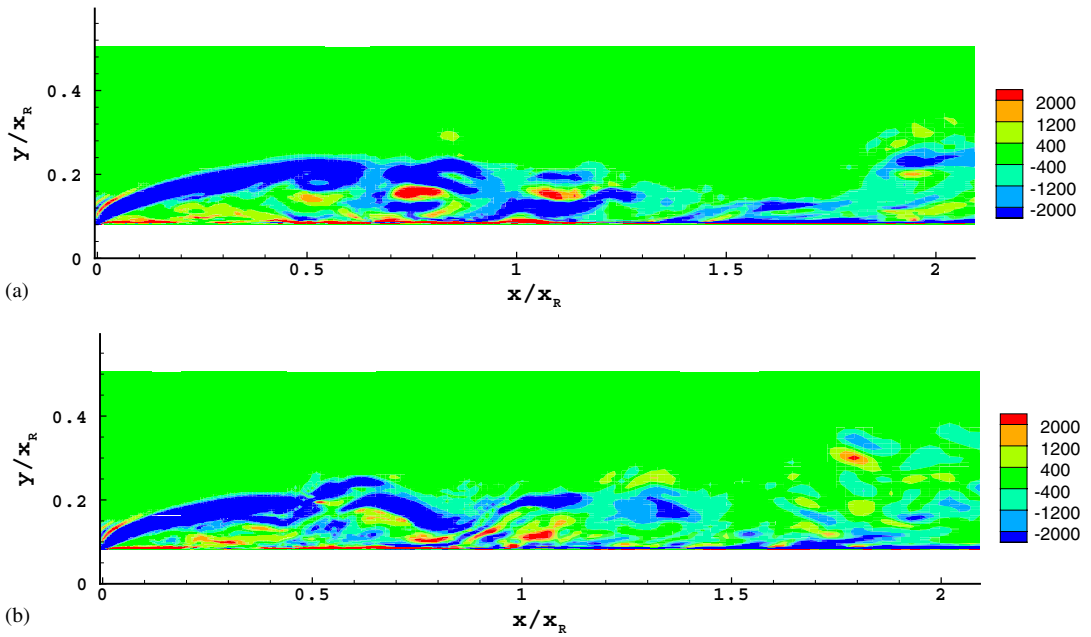

Figure 5. Instantaneous spanwise vorticity: (a) NFST case; and (b) FST case.

the separated boundary layer occurs earlier than in the NFST case. This can be confirmed by Figure 3 which shows that the axial velocity fluctuations rms values in the FST case are bigger than those in the NFST case and closer to the experimental data at the first two streamwise stations. At the leading edge of the plate the flow is still laminar for the FST case and profiles of turbulence rms quantities very close to the leading edge also confirm this.

3.3. *Large-scale structures*

3.3.1. By low-pressure fluctuation isosurfaces. Detailed flow structures for the NFST case have been presented by Abdalla and Yang [17] and some of these structures will be shown here briefly again for comparison with the structures under free-stream turbulence.

The free shear layer becomes unstable due to Kelvin–Helmholtz instability and Kelvin–Helmholtz billows are shed downstream of the plate leading edge and grow in size as they travel downstream. This is clearly demonstrated by Figures 6(a) and (b) which show two spanwise vortex tubes (rolls) visualized by low-pressure fluctuation isosurfaces. The Kelvin–Helmholtz rolls grow in size and are subjected to approximately sinusoidal undulation (waviness) along the spanwise. It can clearly be seen that the axis of the spanwise rolls remains perpendicular to the flow direction thus keeping their coherency and two-dimensionality nature up to this stage. Figures 6(a) and (b) also indicate that as the spanwise waviness develops the peaks and valleys in the successive vortices remain aligned. In transitional terminology this phenomena is called an arrayed pattern. Figures 6(c) and (d) show that the above-described 2D spanwise coherent vortical structures become more distorted (specially the initially shed roll)

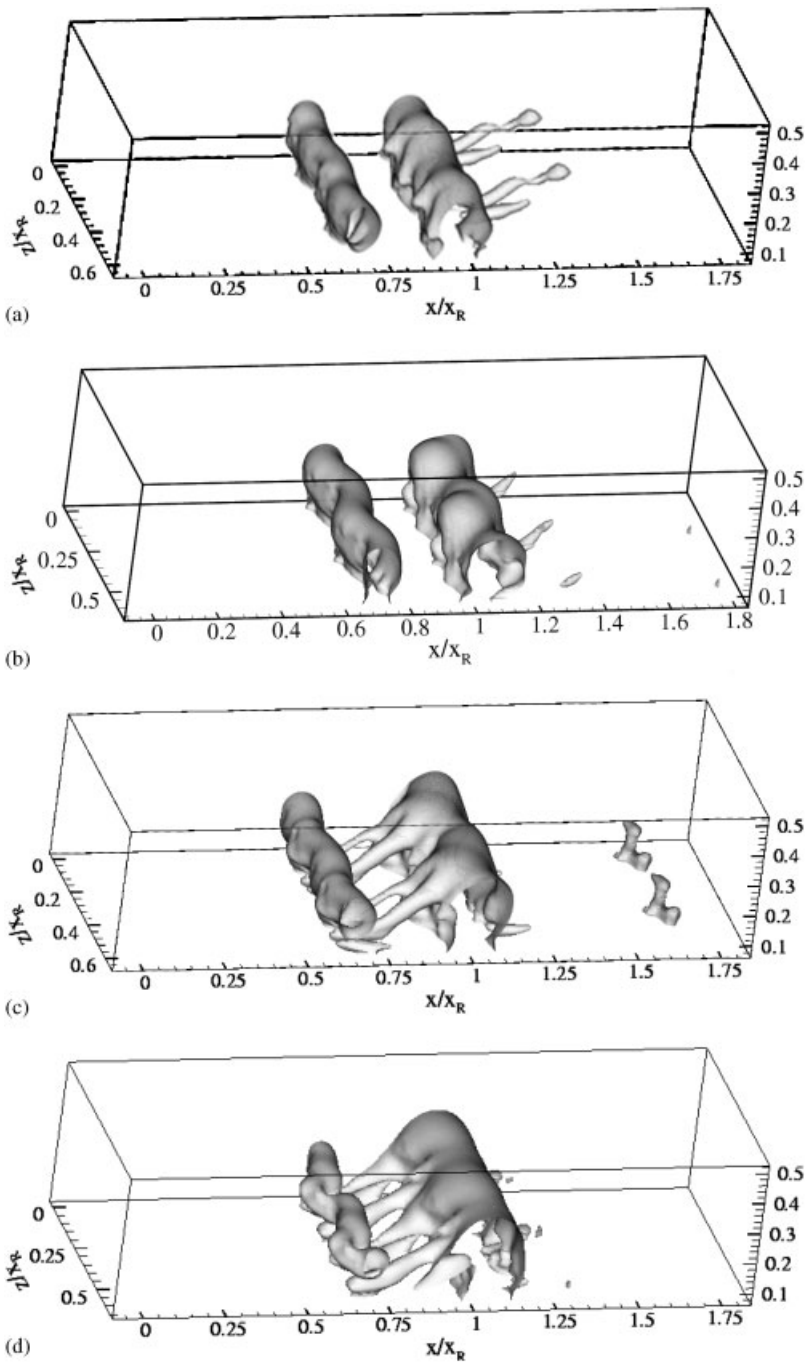

Figure 6. The dominant 2D structures, Kelvin–Helmholtz rolls, and their evolution into streamwise vortical structures visualized by low-pressure isosurfaces: (a) $t = 284.6D/U_0$; (b) $t = 309.1D/U_0$; (c) $t = 348.7D/U_0$; and (d) $t = 356.3D/U_0$.

leading to the appearance of a well-organized array of streamwise vortices originating from the initially shed vortical tube. It is evident that these streamwise vortical structures develop and evolve as a topological consequences of the spanwise oscillation of the Kelvin–Helmholtz billow.

Further investigation on the above-discussed Kelvin–Helmholtz billow reveals that they can develop into Lambda-shaped structures as shown in Figures 7(a) and (b). One can clearly distinguish two sets of Lambda-shaped vortices at different streamwise locations. Very similar structures to those described here were also observed by Suksangpanomrung *et al.* [23] at a much higher Reynolds number (50 000) and by Yanaoka *et al.* [24] at a much lower Reynolds number (450). It is clear that the Kelvin–Helmholtz rolls are transformed into Lambda-shaped vortices. The head of these vortices lie on the original Kelvin–Helmholtz roll while the legs connect the following roll. The Lambda-shaped vortices play an important role in the transition process towards three-dimensionality. Indeed, the Lambda-shaped vortices become part of the core of the spanwise vortex resulting from the pairing of two Kelvin–Helmholtz rolls. As observed by Bernal and Roshko [25] these secondary instabilities (formation of Lambda-shaped vortices) generate the three-dimensionality while pairing redistributes it. This is at the origin of the Kolmogorov energy cascade towards 3D small scales.

Figures 7(c) and (d) show that sometimes the Kelvin–Helmholtz rolls can also evolve into streamwise vortices popularly known as Ribs. The figures clearly show that the Kelvin–Helmholtz rolls have been transformed into streamwise ribs connecting a totally distorted and torn apart spanwise vortical structures. It is quite tempting to assume that these ribs are actually originating from Lambda-shaped vortices which are subjected to more stretching along the axial direction leading to the disintegration of its legs.

It can be concluded for the NFST case from Figures 6 and 7 that distorted 2D structures form before $x/x_R = 0.6$ and evolve into 3D structures after $x/x_R > 0.6$, indicating that the flow has not developed into turbulent flow before $x/x_R < 0.6$. This can be confirmed further by Figure 3 which shows that the predicted axial velocity fluctuations rms values at $x/x_R = 0.6$ are smaller than the turbulent values given by the experimental data as the flow was turbulent in the experiment at this station. Further downstream at $x/x_R = 0.8$ and 1.0, the predicted rms values are more or less the same as the experimental data, supporting what observed in Figures 6 and 7 that distorted 2D structures evolve into 3D structures after $x/x_R > 0.6$ which means that flow develops into turbulent flow.

However, the structures appear to be different under 2% FST as shown in Figure 8 for the FST case. The structures display a more chaotic behaviour compared with the NFST case. The 2D Kelvin–Helmholtz rolls are not as apparent as in the NFST case although a fairly coherent 2D structure in the early part of the bubble can be still observed. The Lambda-shaped vortices, so clearly visible in the NFST case, can hardly be identified in the FST case. Thus, the addition of the FST with magnitude 2% has contaminated and smeared the coherent 2D structures referred to as Kelvin–Helmholtz rolls in the NFST case and transition seems to occur earlier and more rapidly. The presence of fairly coherent 2D spanwise structures suggests that the primary instability of the free shear is still Kelvin–Helmholtz instability in the FST case as in the NFST case. However, the secondary instability in the FST case could be different from that in the NFST case since the Lambda-shaped vortices can hardly be observed.

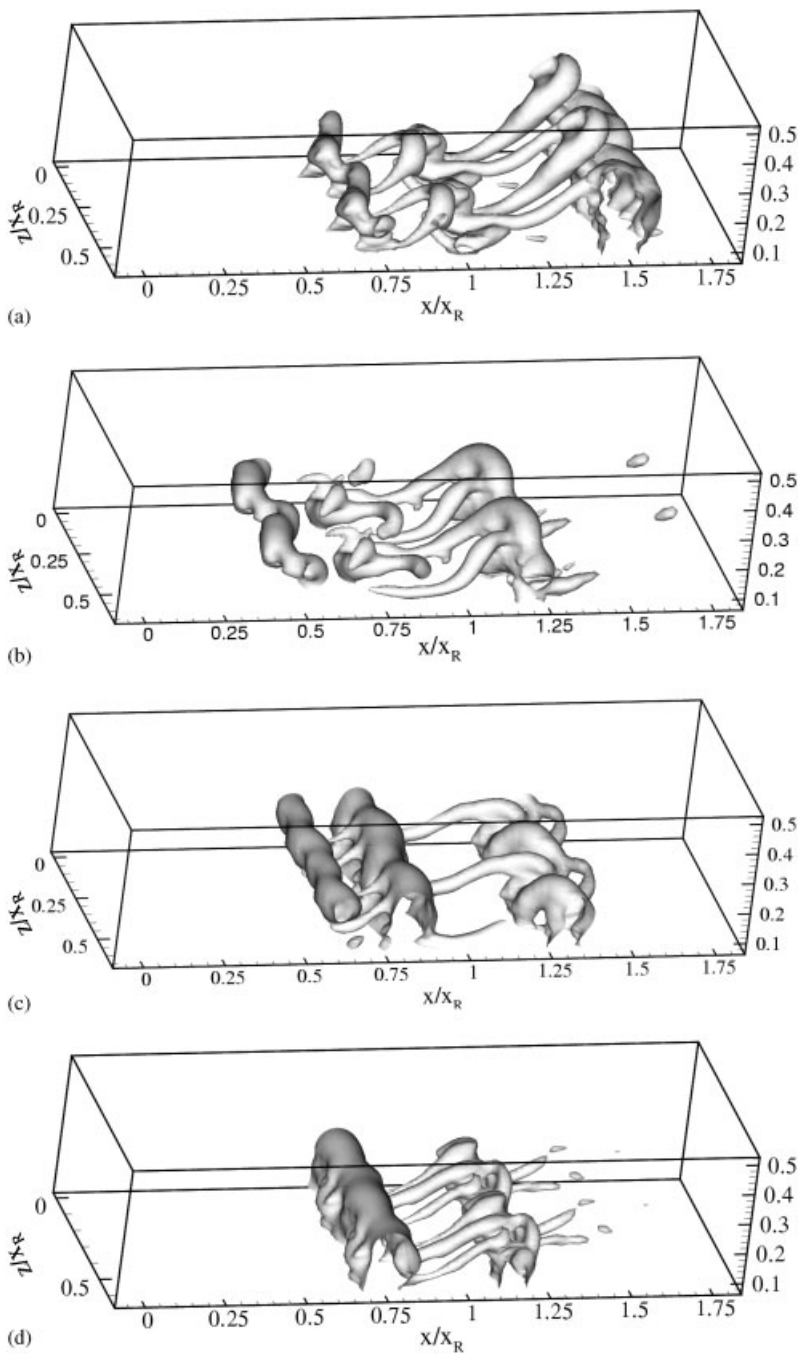

Figure 7. Low-pressure isosurfaces displaying the evolution of the Kelvin–Helmholtz Rolls into the so-called Lambda-shaped vortices (a, b) and the streamwise vortices known as ribs (c, d): (a) $t = 299.7D/U_0$; (b) $t = 348.7D/U_0$; (c) $t = 333.6D/U_0$; and (d) $t = 441D/U_0$.

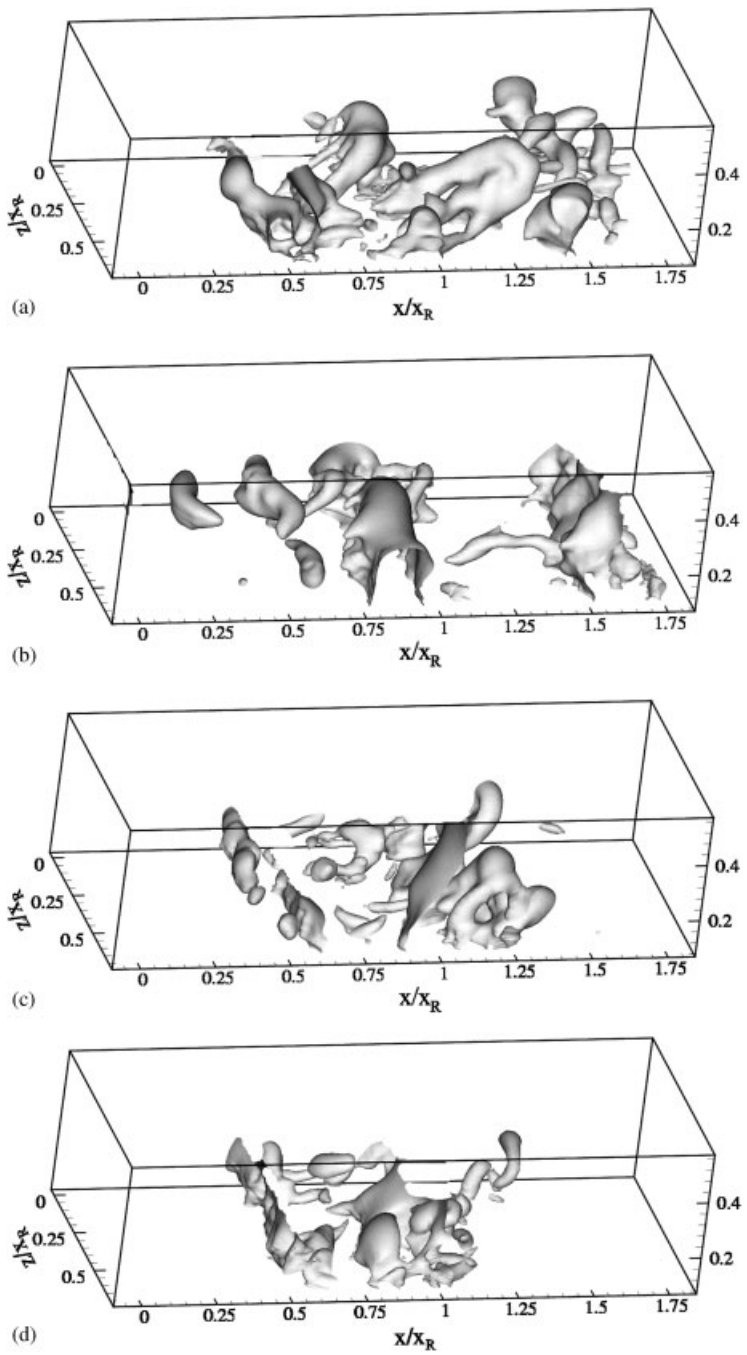

Figure 8. Low-pressure isosurfaces displaying some sort of large-scale structures for the FST case where the so-called Lambda-shaped vortices shown in Figure 7 can hardly be identified: (a) $t = 190.4D/U_0$; (b) $t = 196D/U_0$; (c) $t = 228.1D/U_0$; and (d) $t = 233.7D/U_0$.

3.3.2. By the Q-criterion. This method can be affected by some small noises, which is a common feature. For better and clear results the threshold (maximum value) should be adjusted. The density of structures isolated by the Q-criterion decreases as the threshold increases. The theory behind the visualization method offers no strong basis to support any specific threshold level. Dubief and Delcayre [26] argued that a too large threshold could hide structures, which contribute greatly to high vorticity fluctuation. They added that conditional sampling technique for Q appears to provide valuable hint to a critical threshold value. However, as the main issue in vortex visualization is subjectivity, and since this study is not employing any conditional sampling for any variable involved, the threshold in the current simulation is raised to an extent that the 2D spanwise rolls should not appear and structures smaller than the later can be visualized. The Q-criterion is used in the current study to visualize the evolving small-scale structures resulting from the breakdown of the 2D Kelvin–Helmholtz rolls.

For the NFST case, the extracted vortical structures from the Q-criterion clearly show the evolution of the Kelvin–Helmholtz rolls into well-organized streamwise vortical structures as can be seen in Figures 9(a) and (b). They are usually inclined with a small angle to the axial direction, an indication of larger structures that impinge on the wall. Most likely these structures will suffer some sort of distortion and even breakdown into smaller structures while passing the transition region. However, for the FST case, two distinct features are clear as can be seen in Figures 9(c) and (d). The first feature is that in the NFST case the structures revealed by the Q-criterion are more distinguishable than those appear in the FST case. To be more precise about the word 'distinguishable', one can say that the degree of coherency and organization along both the span and streamwise directions are much obvious in the NFST case compared with the FST case. The second point is that in the NFST case the longitudinal structures are clearly phased along the streamwise direction. In other words, a set of organized longitudinal structures can be observed to evolve in time clearly. A lot of interference between the longitudinal structures along the streamwise is a common feature for the FST case.

Different types of flow have been successfully visualized by using the low-pressure fluctuation isosurfaces and the Q-criterion. Ossia [27] visualized the *worms* structures of isotropic turbulence using DNS data. The Kelvin–Helmholtz billows and the evolving longitudinal structures were successfully visualized in the LES simulation of Comte *et al.* [11] for perturbed mixing layer. The streaky structures and the near-wall Lambda-shaped vortices were also visualized by Lamballais [28]. However, the present study of separated and reattached flow presents several regions with very different characteristics than the flows described above. It is a combination of free shear and wall flows with recirculation zones. This is a severe test for those two visualization methods and it is evident from the above discussion that low-pressure fields can be used to show the structures of larger dimensions better than the structures isolated by the Q-criterion. For a backward-facing step, Delcayre and Lesieur [29] employed the two methods mentioned above. They found that large-scales structures are represented by the low-pressure isosurfaces both upstream and downstream of the reattachment. The current study is consistent with the previous studies.

3.3.3. Vorticity fields. Figure 10(a) shows a snapshot of the instantaneous streamwise vorticity isosurfaces for the NFST case. The streamwise vorticity field indicates that traces of streamwise vorticity exist in the early stages of the flow development (between $x/x_R = 0.25$ and 0.5). The main concentration of the streamwise vorticity is confined to the region around the reattachment ($x/x_R = 0.6$–1.0) where most of the events from transition to turbulence and

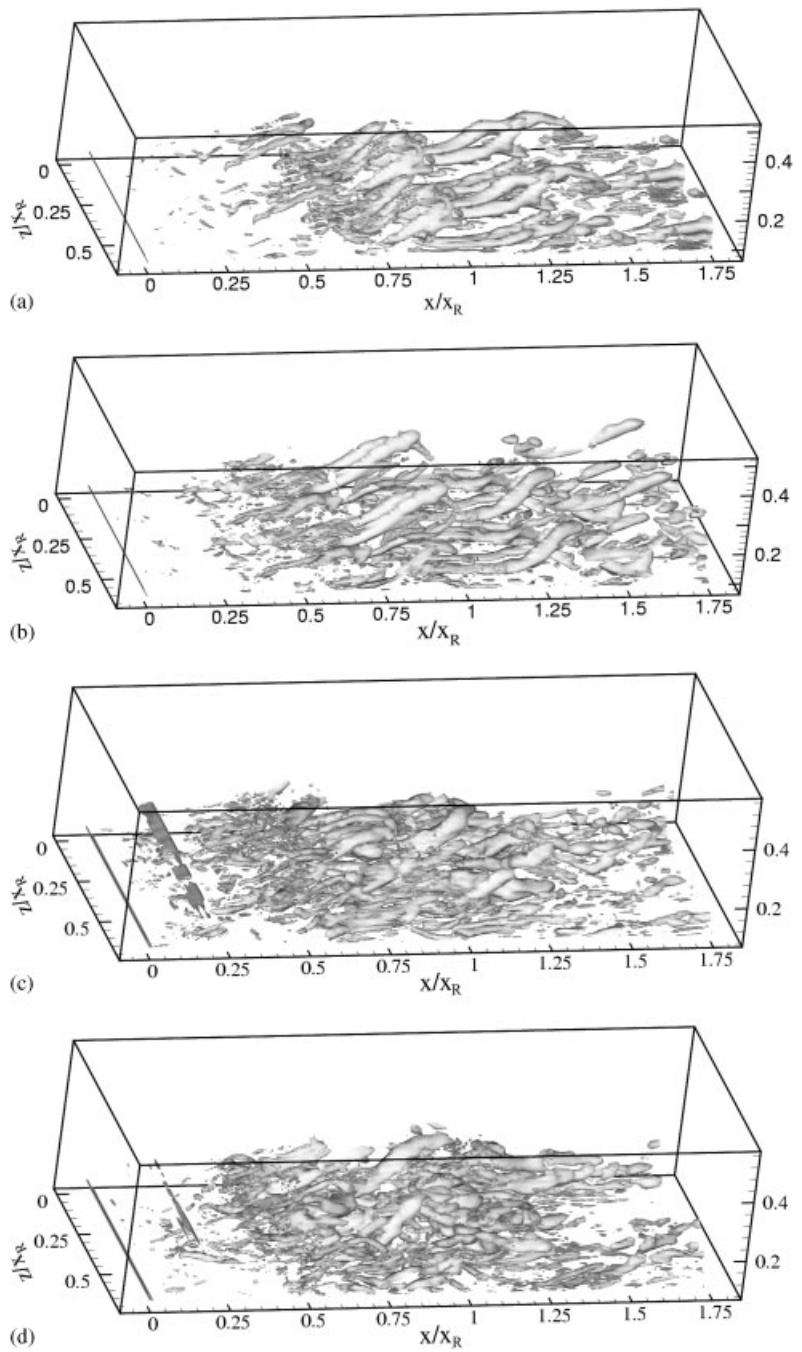

Figure 9. Q-isosurfaces displaying large-scale structures for both the NFST case (a, b) and the FST case (c, d): (a) $t = 319.1D/U_0$; (b) $t = 356.3D/U_0$; (c) $t = 194.2D/U_0$; and (d) $t = 197.9D/U_0$.

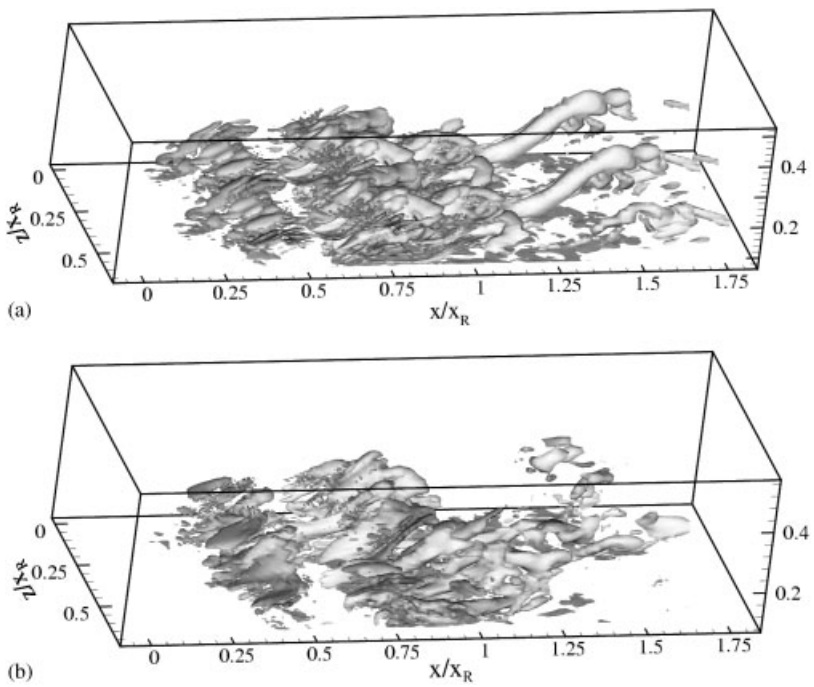

Figure 10. Streamwise vorticity isosurfaces showing large-scale structures for both the: (a) NFST case, $t = 365.7D/U_0$; and (b) FST case, $t = 199.8D/U_0$.

reattachment take place. In this region, streamwise vorticity shows a fairly organized streamwise structures with some distortion visible in the reattachment region. Strong streamwise vortical structures can be seen stretching in the region between $x/x_R = 1.0$ and 1.4. Such streamwise vortical structures might have survived the reattachment region (due to an overriding eddy) and may travel a considerable distance downstream of reattachment before being dissipated into smaller scale turbulent structures. It seems that the evolving streamwise vortical structures are gradually lifted up and become far from the solid wall while stretching along the axial direction. The result is a thinner but stronger longitudinal structure, which might not interact with the wall in the reattachment region. Instead they might interact with smaller scale structures at the turbulent boundary layer forming after reattachment thus leading to a weaker dissipation rate, and hence the probability of survival up to some distance downstream of reattachment. This may explain why the turbulent boundary layer does not develop into a canonical one up to some distance downstream of reattachment as observed by many researchers [30–32]. Figure 10(b) shows a snapshot of the instantaneous streamwise vorticity isosurfaces for the FST case. The main differences are: firstly, the streamwise structures in the FST case are not as distinguishable as in the NFST case. They appear enlarged along the spanwise and quite short along the streamwise axis. Secondly, the degree of organization is quite chaotic in the FST case compared with the NFST case. What is visualized by the Q-criterion is also exhibited by the streamwise vorticity field here.

Figure 11(a) shows a snapshot of the instantaneous spanwise vorticity isosurfaces for the NFST case. It can be seen that a plane sheet of spanwise vorticity appears starting from

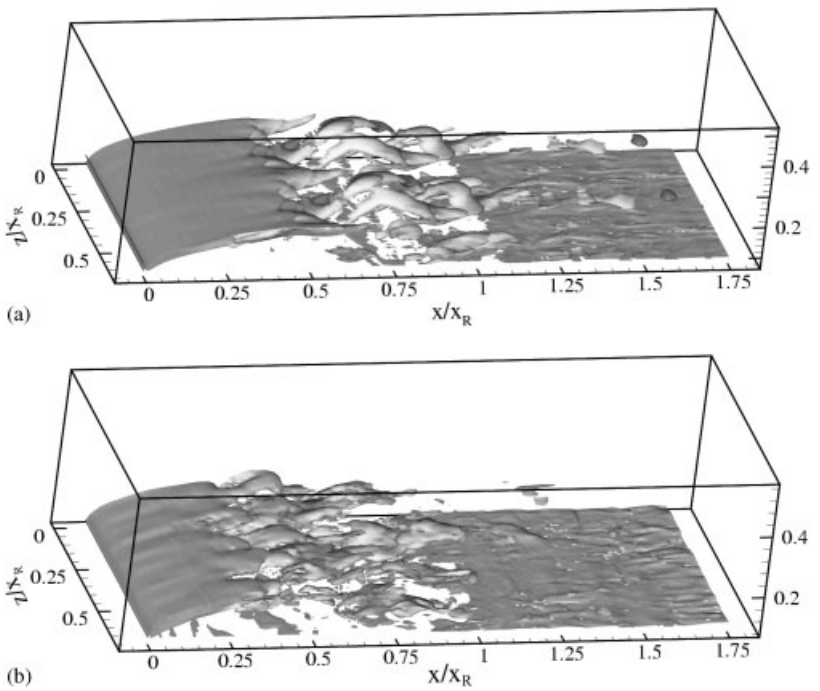

Figure 11. Spanwise vorticity isosurfaces showing large-scale structures for both the: (a) NFST case, $t = 360D/U_0$; and (b) FST case, $t = 192.3D/U_0$.

the leading edge of the blunt plate and begins to disintegrate at around $x/x_R = 0.6$ where 3D motion starts to develop rapidly. Eventually, the vorticity sheet breaks down into intense longitudinal vortical structure covering the region between $x/x_R = 0.5$ and 1.0. Figure 11(b) shows a snapshot of the instantaneous spanwise vorticity isosurfaces for the FST case. Similarly, a plane sheet of vorticity appears starting from the leading edge of the blunt plate. However, it begins to disintegrate much earlier at around $x/x_R = 0.4$, breaking down into longitudinal vortical structures covering the region between $x/x_R = 0.4$ and 1.0. These streamwise vortices are more random (not evenly distributed along the spanwise direction) and they break down into small scales quite rapidly compared with the NFST case. This can be again confirmed by Figure 3 which shows that in the FST case the predicted axial velocity fluctuations rms values are bigger than those in the NFST case upstream at $x/x_R = 0.2$, 0.4 and 0.6. In the FST case the predicted rms values are smaller than the experimental data at only one very upstream station, $x/x_R = 0.2$, and at $x/x_R = 0.4$ the predicted rms values are very close to the measured turbulent values, supporting the conclusion drawn from the flow visualization on the structures evolution that the distorted 2D structures begin to disintegrate much earlier in the FST case at around $x/x_R = 0.4$, breaking down into longitudinal vortical structures covering the region between $x/x_R = 0.4$ and 1.0. Around the reattachment and downstream of the reattachment region the vorticity field in the FST case is dominated by a finer turbulent vortical structures than in the NFST case.

4. CONCLUSION

Large-eddy simulation has been performed to study the transitional flow over a blunt plate held normal to a uniform stream under 2% free-stream turbulence. The LES results compare reasonably well with the available experimental data. The 2% FST level has resulted in 14% reduction in the mean reattachment length compared with the NFST case. This is consistent with most of the experimental work performed on the blunt plate geometry. The transition process leading to breakdown to turbulence and the large-scale structures associated with the flow topology has been proposed and visualized through different visualization methods, mainly the 'low-pressure', 'Q-criterion' and the 'vorticity fields'.

It is evident from the simulation that although large-scale structures are present at different stages in the separated boundary layer transition for the FST case they are not as distinguishable as in the NFST case. Those structures are a result of the transition process and indeed influence the flow topology in the transition region and downstream of reattachment as well. For the FST case the two-dimensional Kelvin–Helmholtz rolls are still observable in the early stage. For the NFST case the Kelvin–Helmholtz rolls grow in size as they travel downstream and are subjected to spanwise waviness which gradually degrades their two-dimensional nature. The streamwise vortices resulting from the transformation of the Kelvin–Helmholtz rolls are noticed to take the form of Lambda-shaped vortices. However, under 2% FST, the Lambda-shaped structures are hardly identified which suggests that the secondary instability at work may be different in the FST case.

For the FST case, the position of the first unsteadiness moves closer to the separation line and gets strongly amplified at about $x/x_R = 0.25$. Generally speaking, the addition of the FST results in increased rate of the randomness of the flow, as expected. Coherency of the early stage structures along the spanwise direction is highly disturbed.

ACKNOWLEDGEMENTS

The computations were carried out on CRAY T3E at Manchester University, funded by EPSRC under the LES-UK2 Consortium.

REFERENCES

1. Cantwell BJ. Organised motion in turbulent flow. *Annual Review of Fluid Mechanics* 1981; **13**:457–515.
2. Townsend AA. *The Structure of Turbulent Shear Flow*. Cambridge University Press: Cambridge, 1956.
3. Corrsin S. Investigation of flow in an axially symmetric heated jet of air. *NACA Adv. Conf. Rep. 3123*, 1943.
4. Brown GL, Roshko A. On density effects and large structure in turbulent mixing layers. *Journal of Fluid Mechanics* 1974; **64**:775–816.
5. Jeong J, Hussain F, Schoppa W, Kim J. Coherent structure near the wall in a turbulent channel flow. *Journal of Fluid Mechanics* 1997; **332**:185–214.
6. Hussain AKMF, Hayakawa M. Eduction of large-scale organised structures in a turbulent plane wake. *Journal of Fluid Mechanics* 1987; **180**:193–229.
7. Hussain AKMF, Melander MV. Understanding turbulence via vortex dynamics. *The Lumely Symposium*: *Studies in Turbulence*. Springer: Berlin, 1991; 158–178.
8. Hussain AKMF. Coherent structures and turbulence. *Journal of Fluid Mechanics* 1986; **173**:303–356.
9. Li H. Identification of coherent structure in turbulent shear flow with wavelet correlation analysis. *Journal of Fluids Engineering* 1998; **120**:778–785.
10. Gordeyev SV, Thomas FO. Coherent structure in the turbulent planar jet. Part 1: extraction of proper orthogonal decomposition eigenmodes and their self-similarity. *Journal of Fluid Mechanics* 2000; **414**:145–194.
11. Comte P, Silvestrini J, Begou P. Streamwise vortices in large-eddy simulation of mixing layers. *European Journal of Mechanics* 1998; **B17**:615–637.

12. Hunt JCR, Wray AA, Moin P. Eddies, stream, and convergence zones in turbulent flows. *Report CTR-S88*, Centre for Turbulence Research, 1988.
13. Saathoff PJ, Melbourne WH. Effects of free stream turbulence on surface pressure fluctuations in a separation bubble. *Journal of Fluid Mechanics* 1997; **337**:1–24.
14. Hillier R, Cherry NJ. The effects of stream turbulence on separation bubbles. *Journal of Wind Engineering and Industrial Aerodynamics* 1981; **8**:49–58.
15. Nakamura Y, Ozono S. The effects of on a separated and reattaching flow. *Journal of Fluid Mechanics* 1987; **178**:447–490.
16. Kalter M, Fernholz HH. The reduction and elimination of a closed separation region by free-stream turbulence. *Journal of Fluid Mechanics* 2001; **446**:271–308.
17. Abdalla IE, Yang Z. Computational visualisation of separated–reattached transitional flow on a blunt plate. *Journal of Flow Visualization and Image Processing* 2004; **11**:1–28.
18. Yang Z, Voke PR. Large-eddy simulation of boundary layer separation and transition at a change of surface curvature. *Journal of Fluid Mechanics* 2001; **439**:305–333.
19. Yang Z, Voke PR. Large-eddy simulation of separated leading-edge flow in general co-ordinates. *International Journal for Numerical Methods in Engineering* 2000; **49**:681–696.
20. Ruth MR, Chen P, Meiburg E. Development of boundary conditions for direct numerical simulation of three-dimensional vortex breakdown phenomena in semi-infinite domains. *Computers and Fluids* 2004; **33**:1225–1250.
21. Kiya M, Sasaki K. Structure of a turbulent separation bubble. *Journal of Fluid Mechanics* 1983; **137**:83–113.
22. Djilali N, Gartshore IS. Turbulent flow around a bluff rectangular plate. Part I: experimental investigation. *Journal of Fluids Engineering* (ASME) 1991; **113**:51–59.
23. Suksangpanomrung A, Djilali N, Moinat P. Large-eddy simulation of separated flow over a bluff rectangular plate. *International Journal of Heat and Fluid Flow* 2000; **21**:655–663.
24. Yanaoka H, Yoshikawa H, Ota T. Numerical simulation of laminar flow and heat transfer over a blunt flat plate in square channel. *Journal of Heat Transfer* (ASME) 1991; **124**:8–16.
25. Bernal LR, Roshko A. Streamwise vortex structure in plane mixing layer. *Journal of Fluid Mechanics* 1986; **170**:499–525.
26. Dubief Y, Delcayre F. On coherent-vortex identification in turbulence. *Journal of Turbulence* 2000; **1**:1–22.
27. Ossia S. La dynamique des echelles infrarouges en turbulence isotrope incompressible. *Ph.D. Thesis*, Institute National Polytecnique de Grenoble, 1996.
28. Lamballais E. Simulation numerrique de la turbulence dans un canal plan tournant. *Ph.D. Thesis*, Institute National Polytecnique de Grenoble, 1996.
29. Delcayre M, Lesieur M. Topological feature in the reattachment region of a backward-facing step. *AFSOR International Conference on DNS and LES*, Ruston, 1997; 1–17.
30. Castro IP, Epik E. Boundary layer development after a separated region. *Journal of Fluid Mechanics* 1998; **374**:91–116.
31. Bradshaw P, Wong FWF. The reattachment and relaxation of a turbulence shear layer. *Journal of Fluid Mechanics* 1972; **52**:327–361.
32. Alving AE, Fernholz HH. Turbulence measurements around a mild separation bubble and downstream of reattachment. *Journal of Fluid Mechanics* 1996; **322**:297–328.

